HHS Public Access

Author manuscript

Retina. Author manuscript; available in PMC 2024 November 01.

Published in final edited form as:

Retina. 2023 November 01; 43(11): 1904–1913. doi:10.1097/IAE.0000000000003881.

Inflammatory cell activity in treated neovascular age-related macular degeneration, a histologic case study

Andreas Berlin, MD, MS[1,2], **Jeffrey D Messinger, DC**[1], **Prithvi Ramtohul, MD**[3], **Chandrakumar Balaratnasingam, MD, PhD**[4,5,6], **Randev Mendis, MD**[7], **Daniela Ferrara, MD, PhD**[8], **K. Bailey Freund, MD**[3,9], **Christine A Curcio, PhD**[1,*]

[1]Department of Ophthalmology and Visual Sciences, Heersink School of Medicine, University of Alabama at Birmingham, Birmingham AL, USA

[2]Department of Ophthalmology, University Hospital Würzburg, Würzburg, Germany

[3]Vitreous Retina Macula Consultants of New York NY, USA

[4]Centre for Ophthalmology and Visual Science, University of Western Australia, Perth, Australia

[5]Lions Eye Institute, Nedlands, Western Australia, Australia

[6]Department of Ophthalmology, Sir Charles Gairdner Hospital, Western Australia, Australia

[7]Canberra Retina Center, Canberra Australia

[8]Genentech, South San Francisco, CA, USA

[9]Department of Ophthalmology, New York University Grossman School of Medicine, New York NY, USA

Abstract

Background—Imaging indicators of macular neovascularization (MNV) risk can help determine patient eligibility for new treatments for geographic atrophy secondary to age-related macular degeneration (AMD). Because type 1 MNV includes inflammation, we assessed by histology the distribution of cells with inflammatory potential in two fellow eyes with AMD.

Methods—Two eyes of a white woman in her 90's with type 3 MNV treated with anti-vascular endothelial growth factor were prepared for high-resolution histology. Eye-tracked spectral-domain optical coherence tomography (OCT) applied to the preserved donor eyes linked *in vivo* imaging to histology. Cells were enumerated in the intraretinal, subretinal and sub-retinal pigment epithelium (RPE)-basal lamina (BL) compartments on 199 glass slides. Cells with numerous

[*]**Corresponding Address** Christine A. Curcio, PhD; Department of Ophthalmology and Visual Sciences; EyeSight Foundation of Alabama Vision Research Laboratories; 1670 University Boulevard Suite 360; University of Alabama at Birmingham, Heersink School of Medicine; Birmingham AL 35294-0099; christinecurcio@uabmc.edu.

Contribution statement

All authors were involved in drafting the article or revising it critically for important intellectual content, and all authors approved the final version to be published. Dr. Curcio and Dr. Berlin had full access to all the data in the clinical picture and take responsibility for the integrity of the data and the accuracy of the data analysis. Study conception and design: CC, KBF, DF, CB, AB. Acquisition of data: RM, CB, JM, AB, DF, KBF, CC. Analysis and interpretation of data: AB, DF, KBF, CC. Writing of manuscript: AB, CB, RM, DF, KBF, CC.

organelles were considered to RPE-derived; cells with sparse RPE organelles were considered non-RPE phagocytes.

Results—Both eyes had soft drusen and abundant SDD. In the retina and subretinal space, RPE-derived cells, including hyperreflective foci, were common (n=125, 73, respectively). Non-RPE phagocytes were infrequent (n=5 in both). Over drusen, RPE morphology transitioned smoothly from the age-normal layer towards the top, suggesting transdifferentiation. The sub-RPE-BL space had RPE-derived cells (n=87) and non-RPE phagocytes (n=49), including macrophages and giant cells.

Conclusions—Numerous sub-RPE-BL cells of several types are consistent with the documented presence of pro-inflammatory lipids in drusen and aged Bruch's membrane. The relatively compartmentalized abundance of infiltrating cells suggests that drusen contents are more inflammatory than SDD, perhaps reflecting their environments. Ectopic RPE occur frequently. Some manifest as hyperreflective foci. More cells may be visible as OCT technologies evolve.

Summary Statement

In two eyes of one patient with anti-VEGF treated type 3 macular neovascularization, histologic analysis revealed many phagocytes (RPE-derived and non-RPE) inside large centrally located drusen and few associated with subretinal drusenoid deposits. The relatively compartmentalized abundance of infiltrating cells suggests that drusen are more inflammatory than subretinal drusenoid deposits.

Keywords

age-related macular degeneration; type 3 macular neovascularization; macrophages; microglia; retinal pigment epithelium; drusen; epithelial mesenchymal transition; subretinal drusenoid deposits; reticular pseudodrusen; optical coherence tomography; histopathology

Introduction

Age-related macular degeneration (AMD) causes legal blindness in older persons worldwide. Macular neovascularization (MNV) affecting 15% of AMD patients is managed by intravitreal injections of anti-vascular endothelial growth factor (VEGF) therapy under guidance from optical coherence tomography (OCT) to reveal layers of retina and choroid. For several reasons, new histology of eyes with MNV, the subject of this report, may help improve diagnosis and management of this common condition.

First, a newly approved treatment for geographic atrophy was associated with a low rate of incident type 1 MNV, possibly due to pre-existing, non-symptomatic neovessels. Figure 1 illustrates an elevation of the retinal pigment epithelium (RPE) containing heterogenous hyperreflective material and lacking flow signal on OCT angiography. Better ways to interpret material between RPE basal lamina and inner collagenous layer of Bruch's membrane (sub-RPE-BL space) in structural OCT may help in assessing risk for future exudation and patient eligibility for new treatments.

Second, new structural OCT technology promises to reveal further details of exudation, MNV, and precursors. Exudative AMD on OCT is characterized by intraretinal, subretinal, and subRPE-BL hyperreflective lesions, representing MNV, and hyporeflective spaces, representing fluid. Figure 1 shows that current spectral domain OCT with 7 μm axial resolution reveals cell-sized features in the sub-RPE-BL space. High-resolution OCT (HR-OCT) with 3 μm axial resolution is expected to show these plus thin layers of basal laminar deposits (BLamD, thickening of RPE-BL material) and basal linear deposits (BLinD, soft drusen material).

Third, new histology may elucidate progression sequences driven by AMD deposits, thus leveraging a large knowledge base for drusen for insights into the more recently recognized subretinal drusenoid deposit (SDD; also called reticular pseudodrusen). Soft drusen are direct precursors to choroidal-originating type 1 MNV. In-growing neovessels replace and/or remove drusen material in the sub-RPE-BL space and ramify along a cleavage plane toward the fovea.[1] SDD associate with type 3 (intraretinal) MNV, sometimes occurring over drusen. Interestingly, type 3 MNV does not occur where SDD start and are most abundant, [2] suggesting that SDD are MNV indicators more than direct precursors.

Type 1 MNV is considered a tissue-healing granulation response to many stimuli, involving phases of inflammation, resolution, and involution.[3] Cellular activity is one indicator of inflammation. Macrophages and other immunocompetent cells are known occupants of the sub-RPE-BL space. [4] Cells also seen around large SDD.[5] In addition to macrophages and microglia with well-studied roles in inflammation, RPE cells may also participate, by leaving the RPE layer, crossing the subretinal space, and entering the retina. This migratory behavior may manifest clinically as hyperreflective foci (HRF), without accounting for all HRF. Some pigmented cells may also localize to the sub-RPE-BL space. Ectopic pigmented cells express immune markers, suggesting molecular transdifferentiation and new functions.[6] Whether these cells are victims, instigators, or responders to other pathology like SDD and type 3 MNV is unknown.

We herein report a histologic analysis of cells in intraretinal, subretinal, and sub-RPE-BL compartments in two fellow eyes with anti-VEGF treated type 3 MNV, monitored by OCT over 5 years. Type 3 MNV evolves in an AMD setting along with soft drusen, HRF, and SDD, as seen in the index case. Thus type 3 MNV offers an entrée to a cellular basis of inflammation in deposit-driven AMD.

Methods

Compliance

This study was approved by Institutional review at the University of Alabama at Birmingham (protocol #300004907) and conducted in accordance with the tenets of the Declaration of Helsinki and the Health Insurance Portability and Accountability Act of 1996.

Clinical course

As described, [7] a white, pseudophakic woman in her 90's received comprehensive ophthalmologic examination and multimodal imaging during a 5-year follow-up. The patient presented in 2014 with exudative type 3 MNV secondary to AMD in the right eye. Significant macular exudation responded well to anti-VEGF therapy but required ongoing treatment. Over 5 years, she received 37 intravitreal anti-VEGF injections over 6 fluid resorption cycles in the right eye. The left eye was diagnosed with exudative type 3 MNV 4 years after the right eye. Over 9 months, the left eye received 6 intravitreal anti-VEGF injections over 2 fluid resorption cycles. General medical history included long-term dyslipidemia and paroxysmal atrial fibrillation. In late 2018 the patient was diagnosed with terminal gallbladder carcinoma (adenocarcinoma). Her last ophthalmic evaluation and anti-VEGF treatment was in January 2019, 2 months before death of adenocarcinoma. Six of 7 vascular lesions were confirmed by histology in these two treated eyes.[7]

Clinical image capture and analysis; tissue preparation for cellular analysis

Detailed methods are found in the Supplementary eMethods. All clinical images were acquired using Spectralis HRA+OCT (Heidelberg Engineering, Heidelberg, Germany). As described, globes were recovered 2:05 hours after death.[8] Post-mortem OCT volumes were captured and registered to pre-mortem OCT volumes of the same globes prior to preparation for high-resolution histology.[9]

We used the eye-tracked OCT scans to enumerate morphologically recognized cell types within subfields of the Early Treatment of Diabetic Retinopathy Study (ETDRS) grid. Attention to regional localization incorporates a new and potentially simplifying concept in AMD pathophysiology. Due to topographic similarity of soft drusen to foveal cones and Müller glia, and SDD to rods, extracellular deposits are proposed as dysregulation of constitutive functions specific to each photoreceptor type.[10]

Deposits, cells, and cellular components are defined in Supplementary eMethods and Supplementary Table 1. Cells with abundant RPE organelles (spindle-shaped melanosomes, lipofuscin, and melanolipofuscin) were considered RPE-derived. Cells with sparse or no RPE organelles were considered non-RPE phagocytes and included morphologically recognizable macrophages, giant cells, and microglia.

Results

Deposits

On 199 glass slides from two eyes, SDD and drusen were present on 199 and 178, respectively. SDD were present inside and outside the ETDRS grid. Large soft or calcified drusen were mainly in the ETDRS central subfield and inner ring. Smaller drusen (soft and nodular) were found throughout the grid. Basal linear deposit (BLinD) extended beyond the large drusen, still within the grid.

Figures 2&3 show clinical images and corresponding histology in regions of drusen at differing stages. Figure 2 shows centrally located, confluent soft drusen. In eyes post-fixed

by osmium tannic acid paraphenylenediamine, native soft drusen have homogeneously gray and textured interiors in light microscopy (Figure 2C1&C2). The bacillary layer overlying these drusen is continuous. Outer segments are shortened or absent. Inner segments over drusen tops are shortened as well. Figure 3A1 shows a druse mostly filled with calcific nodules, one possible end stage of soft drusen. In some drusen, nodules had been partly dislodged by processing. The top of the calcified druse has a patch of photoreceptor atrophy that is delimited on either side by ELM descents. OCT shows a large, calcified druse with thickened RPE next to it (Figure 3A3). By histology cells can be seen to change in a continuous fashion from in-layer to intraretinal. Figure 3B shows a sequence of RPE transdifferentiation along basal laminar deposit (BLamD), from the base of a druse to its apex. In-layer RPE atop thick BLamD at either side of the druse is densely packed with dark-staining granules.

Figure 4 shows clinical images and representative histology in a region of abundant SDD and few drusen. Near infrared reflectance shows that SDD spare the fovea and cover the para- and perifovea (Figure 4A1). OCT B-scans confirm the presence of SDD (Figure 4A2). Histology (Figure 4B) reveals the impact of artifactual retinal detachment on SDD analysis. At three sites (Figure 4B, pink arrowheads, left to right), SDD either remain with RPE, dislodge leaving an empty indentation in the outer segments, or fragment near the outer segments. Figure 4C1–2 shows two stage 3 SDD, each shaped like the tip of an arrow, and both attached to the retina. Photoreceptors atop these SDD are either truncated at the ELM or deflected along the sloping sides of the deposit. These SDD (Figure 4C1–2 insets) contain RPE organelles. One SDD has a nucleated cell and an RPE granule aggregate (inset, Figure 4C1). The other SDD has dispersed granules, and its tip enters the ONL (inset, Figure 4C2), which is thinned. Pale-staining Müller glia in the vicinity contain a few RPE granules.

Cells and cellular material

Table 1 presents counts of cells and cellular fragments (334 total) in both eyes. RPE cells/organelles were predominant in the intraretinal, subretinal, and sub RPE-BL compartments (125, 73, and 87 respectively). Non-RPE phagocytes were sparse in the intraretinal and subretinal compartments (5 in each) and common in the sub RPE-BL space (49). Intraretinal and subretinal RPE cellular components were found across all segments of the ETDRS grid and beyond. Subducted RPE were mainly found in the central subfield and inner ETDRS ring, as were non-RPE phagocytes in this compartment.

Figure 3B shows enlarged spherical or ovoid cells on the sloping sides of a druse displaying lack of polarity, slightly reduced packing density of organelles, and lighter coloration in toluidine blue staining, relative to cells at the druse base. Another non-RPE cell type in the retina is shown in Supplementary Figure 1. Just above the ELM, a tight cluster of RPE organelles around a nucleus is reminiscent of an amoeboid microglial cell.

Figure 5 illustrates non-RPE cells and cellular components in the sub RPE-BL space. The RPE layer is thinned, discontinuous, or conglomerated on top of thick BLamD. Numerous spherical cells packed with light brown-staining lipid droplets are considered foam cells (macrophages). Multi-nucleated giant cells next to soft druse material and calcific nodules are also visible. Corresponding OCT B-scans show a split RPE/BrM complex containing

heterogenous reflectivity within the sub RPE-BL space (Supplementary Figure 2). However, specific OCT signatures corresponding to cells like those in Figure 5 cannot be detected.

Figure 6A&B demonstrate instances of single and grouped subducted cells, of RPE origin. These cells can be distinguished from macrophages and multi-nucleated giant cells in the same compartment, as they are flattened and contain melanin and lipofuscin/ melanolipofuscin granules with a similar range of packing densities as seen in in-layer RPE (Figure 6A). Subducted cells (Figure 6A&B) are distinct from the shedding RPE phenotype (Figure 6C), which releases acellular granule aggregates into the underlying BLamD. In Figure 6C the granule aggregate localizes to a basal mound (of soft drusen material), located between the RPE plasma membrane and the RPE-BL. The granule aggregate is thus in a different tissue compartment from the subducted cells and basal linear deposit just below, in the same panel of Figure 6A&B.

Discussion

Inflammation contributes to the pathogenesis of both non-neovascular AMD and neovascular AMD. By enumerating cells in the intraretinal, subretinal, and sub-RPE-BL compartments of fellow eyes with type 3 MNV, we assessed the inflammatory potential of SDD and soft/ calcified drusen in AMD. We found more cells, and more types of cells, in the sub RPE-BL space than in the subretinal space. Many factors may underlie this differential effect, including processing-related loss of subretinal contents, effect of anti-VEGF, later appearance of SDD than drusen, protective mechanisms inside the blood-retina barrier, composition of deposits, and other factors in the local environment. We also found that the vast majority of sub- and intraretinal cells are RPE-derived, which we ascribe to molecular transdifferentiation in response to ischemia.[6]

We separated cells of RPE origin from non-RPE cells using morphologic criteria. We previously illustrated smooth transitions, within single histologic sections, between in-layer RPE to out-of-layer cells with abundant RPE organelles and without ultrastructural evidence of phagolysosomes indicating prior ingestion. [7, 11] Ectopic RPE cells undergo molecular transdifferentiation, exhibiting gain of immune markers (CD68, CD163) and loss of retinoid markers (RPE65, CRALBP) at the same morphologic transitions. [6, 12] We previously correlated histology to HRF via in vivo and ex vivo OCT imaging and found that appearance of clinical HRF may be preceded by RPE layer disturbance. For non-RPE cells to account for these phenomena, they must match both the organelle content and behavior over time. We note that our criteria represent defensible cut-points on a continuum of variation and are thus not absolute. For example, subducted cells may depigment (Zanzottera et al, Figure 3).[32]

Abundance of infiltrating cells in the sub RPE-BL space (Figure 4) reflects the pro-inflammatory nature of high-risk soft drusen material. This finding aligns with previous reports that pan-retinal drusen from AMD donors (i.e., not confined to those in the central high risk area)[13] can induce inflammasome activation in myeloid and mononuclear cells.[14] In addition, drusen material contains bioactive fragments of complement components C3a and C5a, which induce VEGF expression and predispose to MNV.[15] Moreover, choroidal

endothelial cells respond to C5a to recruit macrophages via Ig superfamily-integrin interactions.[16] Thus, accumulation of drusen might be a chemoattractant for macrophages, resulting in recruitment to the sub RPE-BL space.[17]

In contrast, the subretinal space of the index case showed abundant SDD and few infiltrating non-RPE phagocytes. A clinicopathologic correlation of one case with widespread SDD showed within the subretinal space, RPE organelles, ectopic RPE cell bodies, and cells expressing immune markers.[5] Another histologic survey of 33 SDD-bearing eyes of clinically undocumented donors, arguably at early disease stages, did not report subretinal cells other than ectopic RPE.[1, 6] Anterior migratory behavior by RPE is recognizable clinically as HRF and is thought to represent epithelial-mesenchyme transition, [6] a well-studied concept in development, cancer biology, and proliferative vitreoretinopathy.[6] RPE cells actively maintain an immunosuppressive intraocular environment by secreting inhibitory factors into the subretinal space.[18] This may block the undesirable infiltration of microglia and other mononuclear phagocytes into the bacillary layer and surrounding subretinal space, in healthy retina.[19]

Subretinal non-RPE phagocytes, likely macrophages and microglia, were sparse, due to several possible factors. This compartment is inside the blood-retina barrier, which is intact at least early in disease. Multiple anti-VEGF injections might have suppressed chemoattractant stimuli, however the continued sub RPE-BL inflammation continued under these same conditions. A subretinal immune response might have been borne by RPE-derived cells, as mentioned above. Exudation may have caused disappearance of cells along with SDD. SDD start later in life than drusen,[1] however the index case had AMD for over 5 years. Finally, SDD composition may not be pro-inflammatory.

Good evidence supports high-risk soft drusen material as a direct and potent inflammatory stimulus to type 1 MNV. A well-supported model implicates large apolipoprotein B,E-containing lipoproteins as a major component of soft drusen.[10] Secretion of lipids and apolipoproteins is experimentally achievable by functional RPE cells on a substrate that restricts outward transport.[20] Peroxidized lipids (13(S)-hydroperoxy-9Z,11E-octadecadienoic acid and 7-ketocholesterol) found in aged human BrM and non-human primate drusen are confirmed as pro-inflammatory and pro-angiogenic by injection into rodent eyes.[21] Histologic studies show type 1 MNV dissecting in the sub-RPE-BL space to replace drusen material. [1] In this context, macrophages in the sub-RPE-BL space, including some that differentiate into cells with lipid droplets (Figure 6), are expected.[22] A morphologic sequence consistent with entry of fully pigmented cells into this space has also been demonstrated.[11]

In contrast to drusen a progression sequence from SDD to type 3 MNV is less clear. We herein confirm that cells infiltrate when SDD are tall enough (stage 3) to impact photoreceptor inner segments,[5] suggesting that threshold photoreceptor damage is an inciting stimulus. As this case and one other[5] are both advanced AMD, infiltrating cells are apparently not required to initiate SDD formation. Immunoreactivity for complement factor H and C59,[23] fluid phase and membrane regulators of complement, respectively, has been detected in SDD; it is currently unknown whether SDD also contain inflammatory

lipids. More tissue-level assays of SDD composition, e.g., immunohistochemistry and imaging mass spectrometry, are needed. Type 3 MNV occurs closer to the fovea than SDD themselves, as does early visual dysfunction. This spatial disassociation suggests that SDD are a marker for another process, such as choroidal thinning and microvascular insufficiency.

Finally, the local environment may differentially affect the inflammatory potential of drusen and SDD. Oxidatively modified lipids contribute directly to tissue injury or indirectly via oxidation-specific epitopes.[24] Mitochondria are considered the source of 90% of reactive oxygen species in mammalian cells, due to inefficiencies in the electron transport chain. [25] Lipid hydroperoxides are created when reactive oxygen species react with polyunsaturated fatty acids like those in drusen.[26] Of note drusen are several micrometers away from hundreds of mitochondria in the basal RPE cell body,[27] and RPE mitochondrial DNA is damaged in AMD.[28] In contrast, SDD starts far from mitochondria of both RPE and photoreceptor inner segments, at the apical RPE.

Study strengths include a clinically well-documented case, the availability of eye-tracked OCT imaging, a short death-to-preservation interval that largely maintained retinal attachment, and histologic and photomicroscopy techniques that reveal tissue elements comprehensively for comparison to OCT (as opposed to selective stains). Limitations include the lack of immunohistochemistry to support cell type identifications based on morphologic criteria. Artifactual retinal detachment might have dislodged subretinal cells as well as SDD (Figure 4) but would have affected all cell types equally. Further, we presented compartment-level cellular frequencies rather than requiring histologic contiguity with SDD, which were localized from clinical imaging. Finally, data from one patient only cannot elucidate the range of biologic variability, despite being consistent with other descriptions.

In conclusion, we report cells in the retinal, subretinal, and sub-RPE-BL compartments as a measure of inflammation that may confer risk for MNV. Based on the abundance, type, and inferred activity of observed infiltrating cells, we suggest that drusen have a higher inflammatory potential than SDD. Because RPE are not seen to enter SDD but rather crossing it en route to retinal vessels, we also suggest that the initiating stimuli for RPE migration is less inflammation than ischemia and dysmetabolism. Our findings contrast with those in mouse models, including aged wild-type animals, in which resident microglia populate the subretinal space. Species differences are relevant to the interpretation of pre-clinical data. Our analysis represents a proof-of-concept for using the knowledge base for drusen and type 1 MNV to learn about processes relevant to SDD-driven AMD. Looking forward, we expect new OCT technologies to provide further insight into inflammatory cell activities in living persons.

Supplementary Material

Refer to Web version on PubMed Central for supplementary material.

Acknowledgments

Financial support

This work was supported by Genentech/ Hoffman LaRoche, The Macula Foundation, Inc., New York, NY; Dr. Werner Jackstädt-foundation (AB); unrestricted funds to the Department of Ophthalmology and Visual Sciences (UAB) from Research to Prevent Blindness, Inc., and EyeSight Foundation of Alabama. Purchase of the slide scanner was made possible by the Carl G. and Pauline Buck Trust.

The sponsors had no role in the design and conduct of the study; collection, management, analysis, and interpretation of the data; preparation, review, or approval of the manuscript; and decision to submit the manuscript for publication.

Financial disclosure

KBF is a consultant to Genentech, Zeiss, Heidelberg Engineering, Allergan, Bayer, and Novartis. CAC receives research funds from Genentech/ Hoffman LaRoche, Regeneron, Heidelberg Engineering (outside this project) and is a consultant to Astellas, Apellis, Boehringer Ingelheim, Character Bio, and Osanni. DF is an employee of Genentech and a stockholder of Roche.

Meeting presentation

This work was presented at the FLORretina/ ICOOR meeting Rome, 2022.

Abbreviations

AMD	age-related macular degeneration
BL	basal lamina
BLamD	basal laminar deposit
BLinD	basal linear deposit
BrM	Bruch’s membrane
ChC	choriocapillaris
Ch	choroid
ELM	external limiting membrane
GCL	ganglion cell layer
HFL	Henle fiber layer
INL	inner nuclear layer
IPL	inner plexiform layer
IS	inner segment
MA	macular atrophy
MNV	macular neovascularization
OCT	optical coherence tomography
ONL	outer nuclear layer

OPL	outer plexiform layer
OS	outer segment
RPE	retinal pigment epithelium
SDD	subretinal drusenoid deposits
VEGF	vascular endothelial growth factor

References

1. Chen L et al. Biometrics, Impact, and Significance of Basal Linear Deposit and Subretinal Drusenoid Deposit in Age-Related Macular Degeneration. Investigative Ophthalmology & Visual Science 2021; 62:33–33.
2. Haj Najeeb B et al. The RAP study, report 4: morphological and topographical characteristics of multifocal macular neovascularization type 3. Graefe's Archive for Clinical and Experimental Ophthalmology 2022; 260:141–147.
3. Grossniklaus HE and Green WR. Choroidal neovascularization. American Journal of Ophthalmology 2004; 137:496–503. [PubMed: 15013874]
4. Grossniklaus HE et al. Macrophage and retinal pigment epithelium expression of angiogenic cytokines in choroidal neovascularization. Mol Vis 2002; 8:119–126. [PubMed: 11979237]
5. Greferath U et al. Correlation of histologic features with in vivo imaging of reticular pseudodrusen. Ophthalmology 2016; 123:1320–1331. [PubMed: 27039021]
6. Cao D et al. Hyperreflective foci, optical coherence tomography progression indicators in age-related macular degeneration, include transdifferentiated retinal pigment epithelium. Investigative Ophthalmology & Visual Science 2021; 62:34–34.
7. Berlin A et al. Histology of type 3 macular neovascularization and microvascular anomalies in treated age-related macular degeneration: a case study. Ophthalmology Science 2023; 3:100280.
8. Balaratnasingam C et al. Comparisons between histology and optical coherence tomography angiography of the periarterial capillary-free zone. American Journal of Ophthalmology 2018; 189:55–64. [PubMed: 29470970]
9. Litts KM et al. Clinicopathological correlation of outer retinal tubulation in age-related macular degeneration. JAMA Ophthalmology 2015; 133:609–612. [PubMed: 25742505]
10. Curcio CA. Soft drusen in age-related macular degeneration: biology and targeting via the oil spill strategies. Investigative Ophthalmology & Visual Science 2018; 59:AMD160-AMD181.
11. Zanzottera EC et al. Subducted and melanotic cells in advanced age-related macular degeneration are derived from retinal pigment epithelium. Investigative Ophthalmology & Visual Science 2015; 56:3269–3278. [PubMed: 26024109]
12. Augustin S et al. Melanophages give rise to hyperreflective foci in AMD, a disease-progression marker. Journal of Neuroinflammation 2023; 20:1–19. [PubMed: 36593485]
13. Wang JJ et al. Ten-year incidence and progression of age-related maculopathy: the blue Mountains Eye Study. Ophthalmology 2007; 114:92–98. [PubMed: 17198852]
14. Marneros AG. Role of inflammasome activation in neovascular age-related macular degeneration. FEBS J. 2023; 290(1):28–36. [PubMed: 34767301]
15. Nozaki M et al. Drusen complement components C3a and C5a promote choroidal neovascularization. Proceedings of the National Academy of Sciences 2006; 103:2328–2333.
16. Skeie JM et al. Complement component C5a activates ICAM-1 expression on human choroidal endothelial cells. Investigative Ophthalmology & Visual Science 2010; 51:5336–5342. [PubMed: 20484595]
17. Rodriguez IR et al. 7-ketocholesterol accumulates in ocular tissues as a consequence of aging and is present in high levels in drusen. Experimental Eye Research 2014; 128:151–155. [PubMed: 25261634]

18. Zamiri P, Sugita S and Streilein JW. Immunosuppressive properties of the pigmented epithelial cells and the subretinal space. Immune Response and the Eye 2007; 92:86–93.
19. Sennlaub F et al. CCR 2+ monocytes infiltrate atrophic lesions in age-related macular disease and mediate photoreceptor degeneration in experimental subretinal inflammation in Cx3cr1 deficient mice. EMBO Molecular Medicine 2013; 5:1775–1793. [PubMed: 24142887]
20. Hood EM, Curcio CA and Lipinski D. Isolation, culture, and cryosectioning of primary porcine retinal pigment epithelium on transwell cell culture inserts. STAR protocols 2022; 3:101758.
21. Amaral J et al. 7-Ketocholesterol induces inflammation and angiogenesis in vivo: a novel rat model. PloS One 2013; 8:e56099.
22. Grossniklaus HE et al. Correlation of histologic 2-dimensional reconstruction and confocal scanning laser microscopic imaging of choroidal neovascularization in eyes with age-related maculopathy. Archives of Ophthalmology 2000; 118:625–629. [PubMed: 10815153]
23. Rudolf M et al. Sub-retinal drusenoid deposits in human retina: organization and composition. Experimental Eye Research 2008; 87:402–408. [PubMed: 18721807]
24. Handa JT et al. Lipids, oxidized lipids, oxidation-specific epitopes, and Age-related Macular Degeneration. Biochimica et Biophysica Acta (BBA)-Molecular and Cell Biology of Lipids 2017; 1862:430–440. [PubMed: 27480216]
25. Tirichen H et al. Mitochondrial reactive oxygen species and their contribution in chronic kidney disease progression through oxidative stress. Frontiers in Physiology 2021:398.
26. Le N-A. Lipoprotein-associated oxidative stress: a new twist to the postprandial hypothesis. International Journal of Molecular Sciences 2014; 16:401–419. [PubMed: 25548897]
27. Pollreisz A et al. Atlas of human retinal pigment epithelium organelles significant for clinical imaging. Investigative Ophthalmology & Visual Science 2020; 61:13–13.
28. Atilano SR et al. Low frequency mitochondrial DNA heteroplasmy SNPs in blood, retina, and [RPE+ choroid] of age-related macular degeneration subjects. Plos One 2021; 16:e0246114.
29. Chen L et al. Histology and clinical imaging lifecycle of black pigment in fibrosis secondary to neovascular age-related macular degeneration. Experimental Eye Research 2022; 214:108882.
30. Berlin A et al. Correlation of Optical Coherence Tomography Angiography of Type 3 Macular Neovascularization With Corresponding Histology. JAMA Ophthalmol. 2022 Jun 1;140(6):628–633. [PubMed: 35446357]

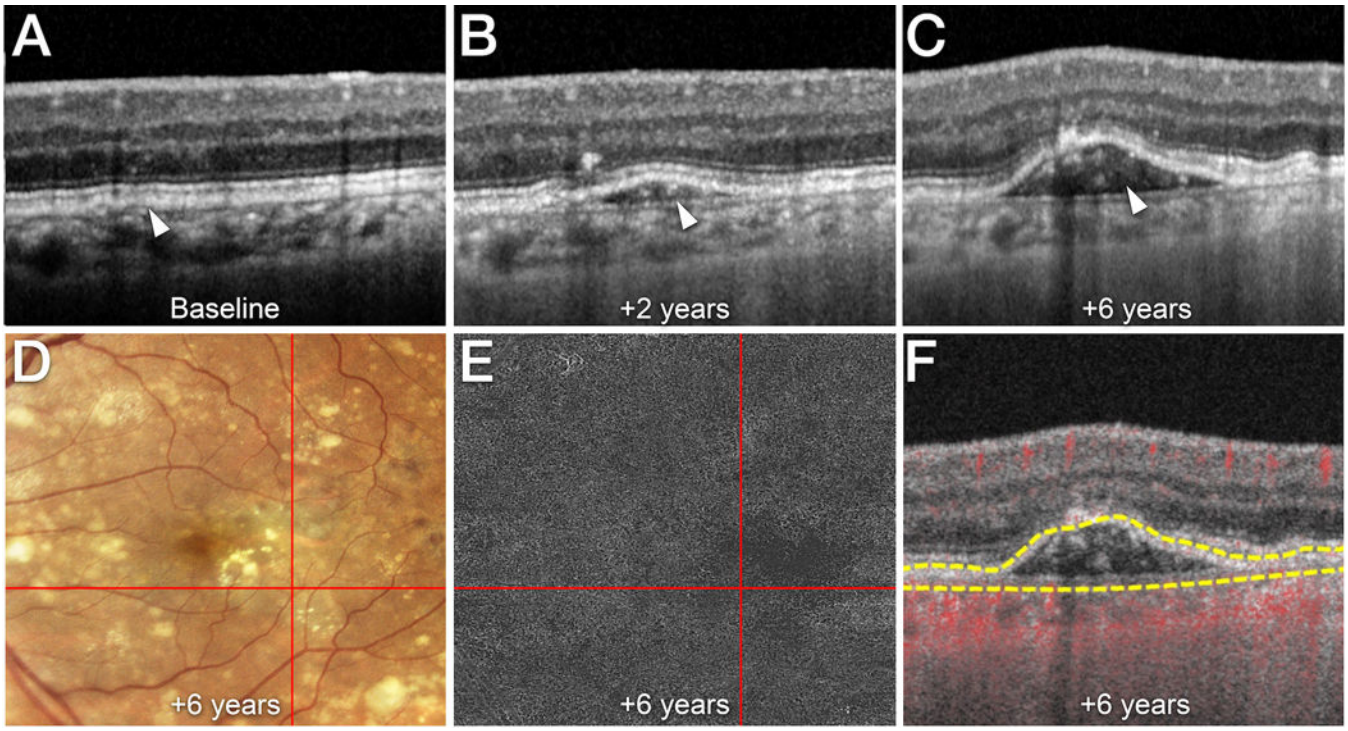

Figure 1. Hyperreflective non-neovascular material in an elevation of the retinal pigment epithelium (RPE).

A-F. Time point after baseline is indicated. A left eye of a male patient in his late 60's followed for non-neovascular AMD is shown.

A Cross-sectional optical coherence tomography (OCT) B-scan (Spectralis, Heidelberg Engineering, Heidelberg, Germany) acquired at baseline shows that the RPE/Bruch's membrane complex is slightly separated by a hyporeflective layer (*white arrowhead*). **B** At 2 years, the retinal pigment epithelium (RPE) is elevated (*white arrowhead*). Note the heterogeneous, hyperreflective material within the sub-RPE/BL space. **C** At 6 years, more hyperreflective material is seen in the sub-RPE/BL space (*white arrowhead*). **D** Confocal color photography (EIDON AF, Centervue Padova, Italy) shows the RPE elevation (*intersection of red lines*) and soft drusen. ***E*** *En face* swept source OCT angiography (SS-OCTA; PLEX Elite 9000, Carl Zeiss Meditec, Inc, Dublin, CA)) segmented at the level of the sub-RPE/BL space (*top line*: RPE / *bottom line*: Bruch's membrane) does not show macular neovascularization within the RPE elevation (*intersection of red lines*). **F** Cross-sectional SS-OCTA with flow signal overlay shows the avascular nature of the sub-RPE/BL hyperreflective material. Yellow lines indicate the segmentation lines used for (**B**).

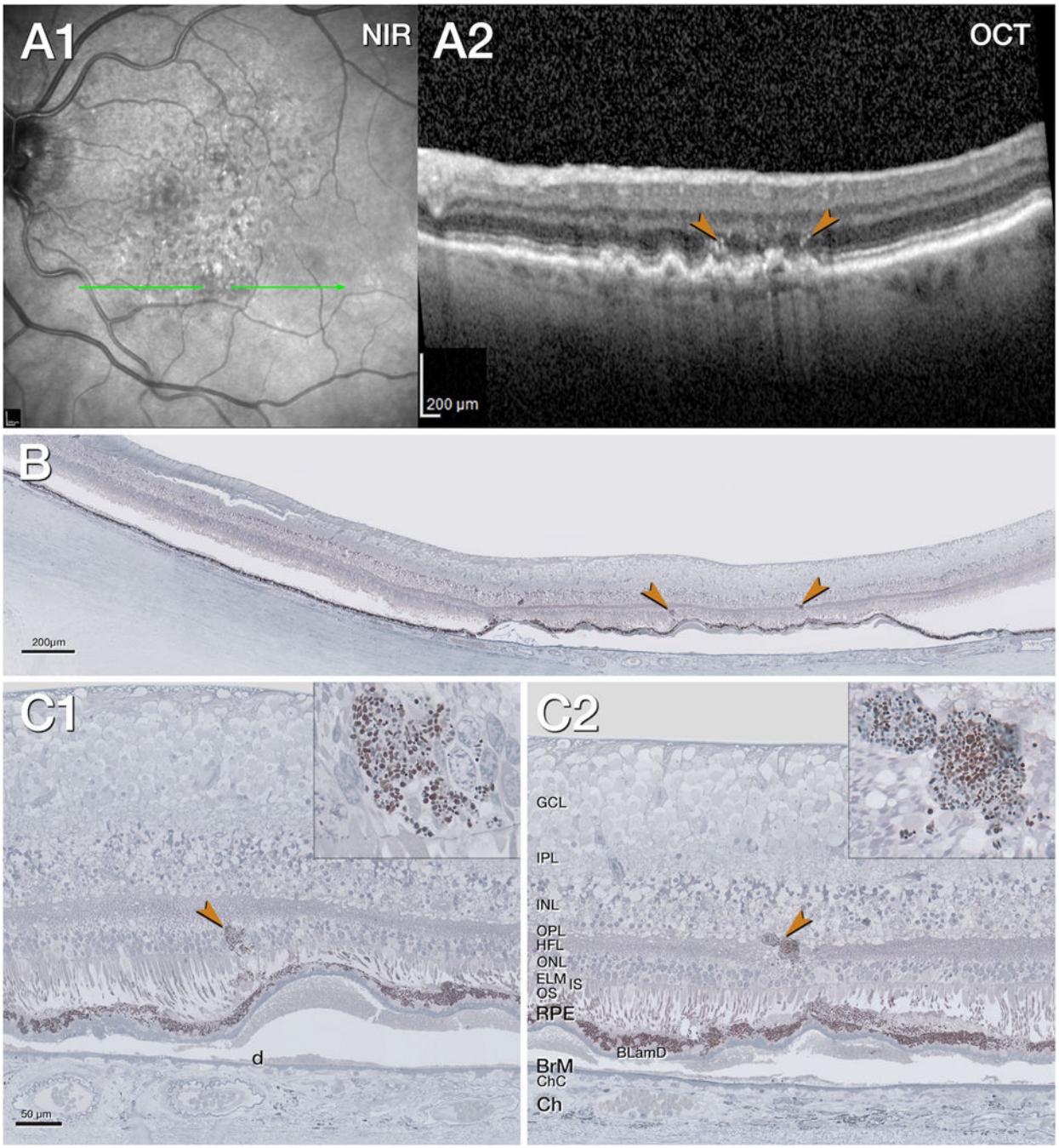

Figure 2. Intraretinal retinal pigment epithelium associated with native soft drusen.

A1. Near infrared reflectance (NIR) shows subretinal drusenoid deposits especially in the superior macula, 11 months before death. The green arrow shows the location and orientation of the optical coherence tomography (OCT) B-scans and histology section. **A2**. The OCT B-scan shows confluent soft drusen with moderately reflective interiors, hyperreflective foci (HRF, brown arrowheads) above a retinal pigment epithelium (RPE) elevation, split RPE/Bruch's membrane (BrM) complex. The choroid is thinned. **B**. Panoramic histology view shows atrophy of the outer retina in the center above several RPE

elevations. The choroid is atrophic. The retina is artificially detached due to histologic tissue processing. The brown arrowheads correspond to hyperreflective foci (HRF) in panel **A2. C1, C2**. Magnified histology shows intraretinal RPE (brown arrowhead, **C1**). One organelle conglomeration (brown arrowhead, **C2**) is next to a vessel in the inner nuclear layer (INL)/ Henle fiber layer (HFL). It is located above an altered RPE layer, separated by basal laminar deposits (BLamD) from the underlying soft druse (d). Insets show different density, and shape, size of RPE organelles.

BLamD, basal laminar deposit; BrM, Bruch's membrane; Ch, choroid; ChC, choriocapillaris; ELM, external limiting membrane; GCL, ganglion cell layer; HFL, Henle fiber layer; INL, inner nuclear layer; IPL, inner plexiform layer; IS, inner segments; NIR, near infrared reflectance; OCT, optical coherence tomography; ONL, outer nuclear layer; OPL, outer plexiform layer; OS, outer segments; RPE, retinal pigment epithelium.

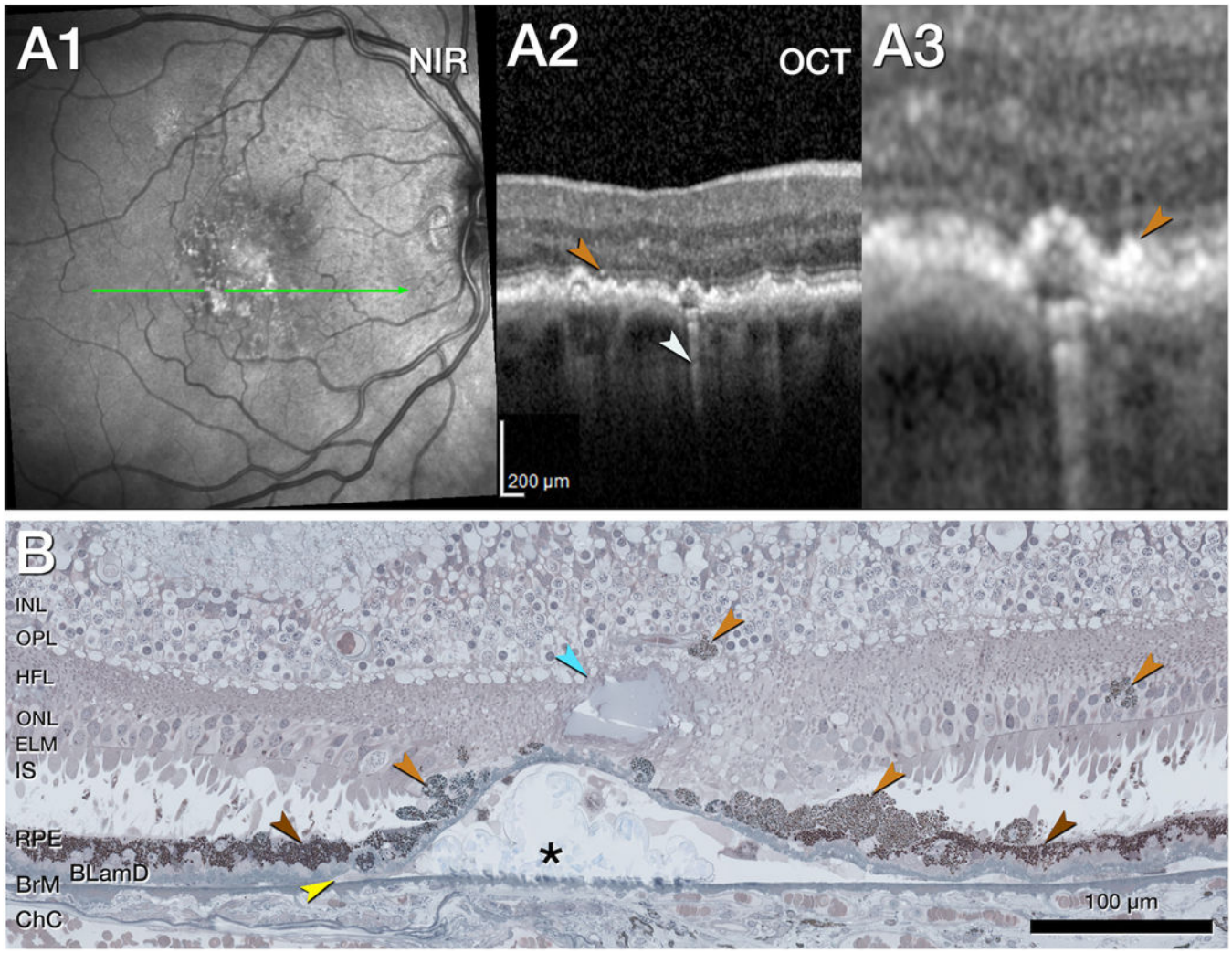

Figure 3. Transdifferentiation of retinal pigment epithelium over a calcified druse

A1. Near infrared reflectance (NIR, **A1**) shows subretinal drusenoid deposits especially in the superior macula, 11 months before death. The green arrow shows the location and orientation of the optical coherence tomography (OCT) B-scans and histology section. **A2**. The OCT B-scan shows retinal pigment epithelial (RPE) elevations with one HRF (light brown arrowhead) and choroidal hypertransmission (white arrowhead). **A3**. Magnified OCT shows a thickened RPE band (light brown arrowhead). **B**. Magnified histology shows the continuous change of RPE cells from in layer cells to transdifferentiated out-layer, sloughed RPE cells over the edge of a druse below an ELM descent and degenerative cysts (dark, light brown, and light blue arrowheads, respectively). While the in-layer RPE cells are largely intact (dark brown arrowheads) on both sides of the druse, and over the edges of the druse, the sloughed RPE cells are disintegrated and stacked (2 lower light brown arrowheads). These RPE differ in shape, size, and reflectivity. Cells are spherical or round and appear lighter in color due to less dense organelle packing density. Migrated RPE cells (2 upper light brown arrowheads) are present in the outer nuclear layer (ONL) and inner nuclear layer (INL) next to a vessel of the deep capillary plexus. Basal laminar deposits (BLamD) and

basal linear deposits (BLinD, yellow arrowhead) separate the RPE from the drusen contents and Bruch's membrane, which is thinned but intact. The choroid appears atrophic. BLamD, basal laminar deposit; BLinD, basal linear deposits; BrM, Bruch's membrane; ChC, choriocapillaris; ELM, external limiting membrane; HFL, Henle fiber layer; INL, inner nuclear layer; IPL, inner plexiform layer; IS, inner segments; NIR, near infrared reflectance; OCT, optical coherence tomography; ONL, outer nuclear layer; OPL, outer plexiform layer; RPE, retinal pigment epithelium.

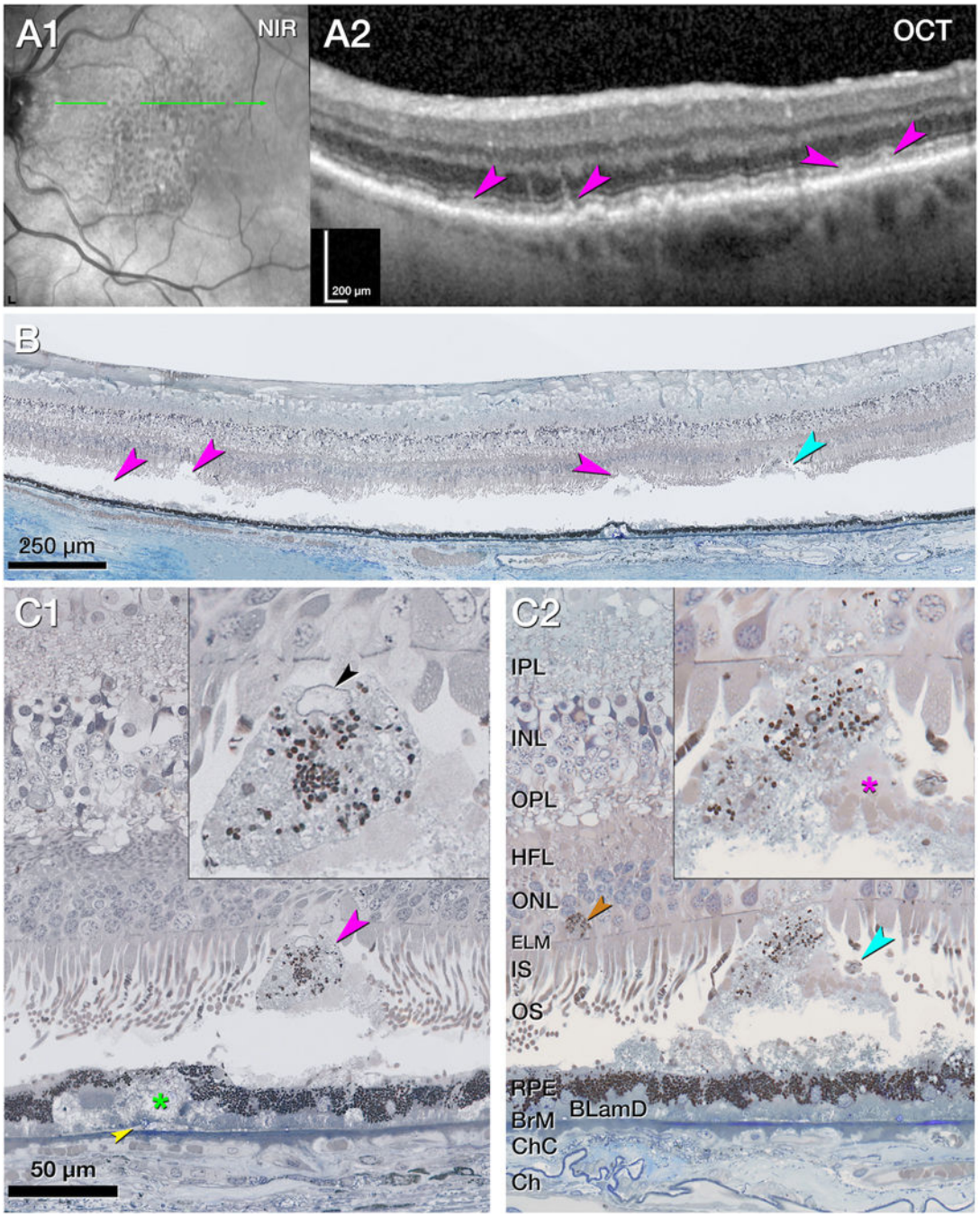

Figure 4. Cells associated with stage 3 subretinal drusenoid deposits

A1. Near infrared reflectance (NIR) shows subretinal drusenoid deposits (SDD) across the superior and central macula, 11 months before death. The green arrow corresponds to the region and orientation of the optical coherence tomography (OCT) B-scans and histology section. Illustrated SDD are representative of a region with numerous SDD. Due to the many deposits and use of stepped sections, it was not possible to match OCT and histology identically. **A2**. The OCT B-scan shows several SDDs (pink arrowheads) next to shallow retinal pigment epithelium (RPE) elevations. The choroid is thinned. **B**. Panoramic histology

view corresponding to an adjacent area of the OCT scan shows 3 sites of artifactual retinal detachment associated with SDD (pink arrowheads). A site of where SDD is attached to the retina (cyan arrowhead) is magnified in panel **C2. C1&2**. Magnified histology with insets shows two stage 3 SDD (pink arrowheads), attached to the photoreceptors and containing RPE organelles. Retinal detachment was digitally re-approximated. The SDD in **C1** came from a section located inferior to panel **B**. The SDD in **C2** is indicated in panel **B**. Photoreceptors atop stage 3 SDDs are truncated at the external limiting membrane (ELM) or deflected along the sides. In **C1** the SDD contains a cell with nucleus (black arrowhead) and an RPE organelle aggregate; this cell is considered a non RPE-phagocyte. Basal mound, BLinD (green asterisk and yellow arrowhead, respectively **C1**), and BLamD separate the RPE from Bruch's membrane (BrM), which is thinned but intact. In **C2** an SDD tip enters into the ONL. Photoreceptor outer segment (OS) fragments appear on one side of the SDD (pink asterisk, inset **C2**). A migrated RPE cell next to a DCP vessel appears next to the SDD (light brown asterisk, **C2**)

BLamD, basal laminar deposit; BLinD, basal linear deposits; BrM, Bruch's membrane; Ch, choroid; ChC, choriocapillaris; ELM, external limiting membrane; HFL, Henle fiber layer; INL, inner nuclear layer;

IPL, inner plexiform layer; IS, inner segments; NIR, near infrared reflectance; OCT, optical coherence tomography; ONL, outer nuclear layer; OPL, outer plexiform layer; OS, outer segments; RPE, retinal pigment epithelium.

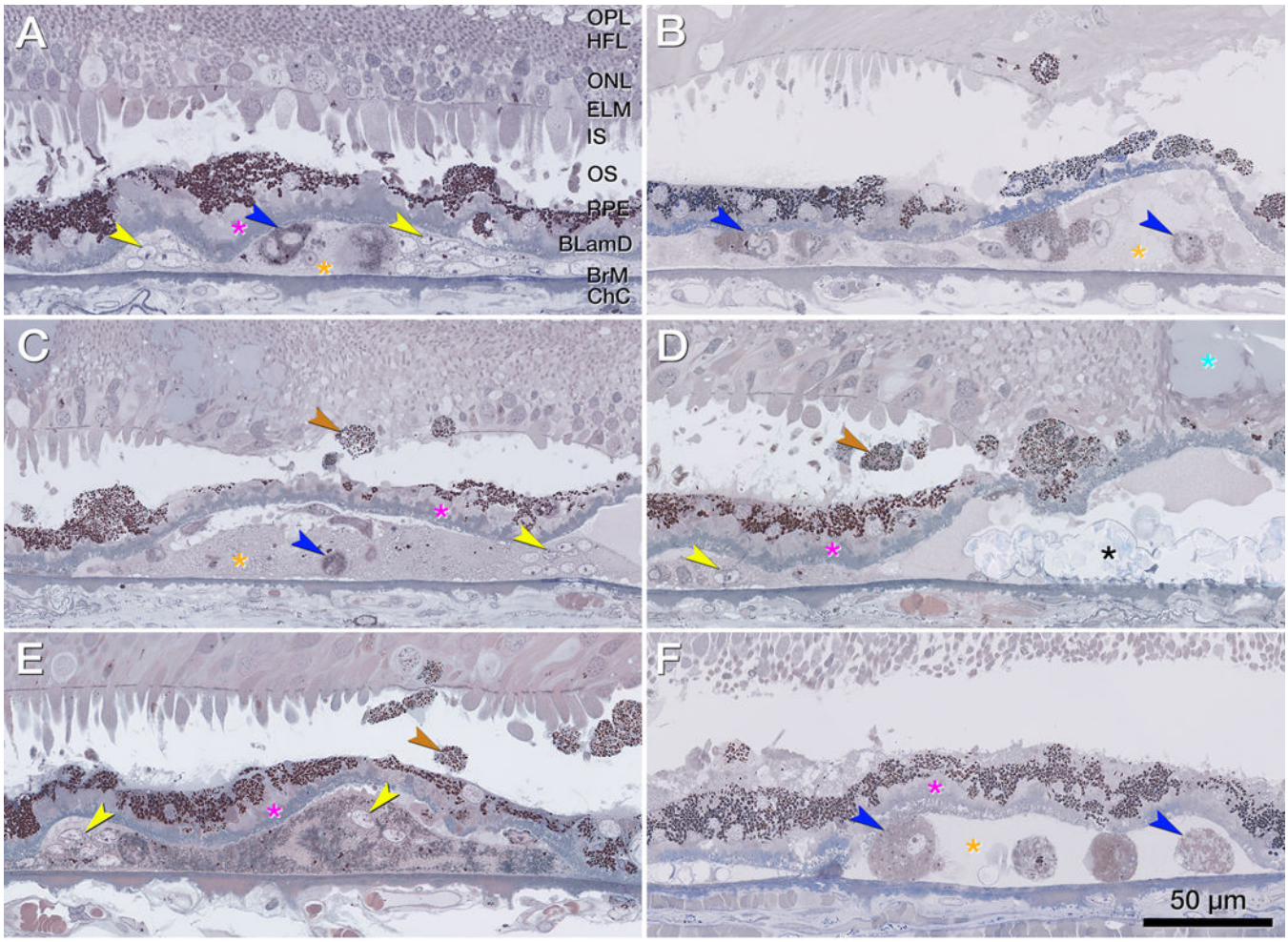

Figure 5. Non-retinal pigment epithelium phagocytes in the sub retinal pigment epithelium basal laminar space.

A-F. Magnified histology shows a split retinal pigment epithelium (RPE)/ Bruch's membrane (BrM) complex with cellular components in its sub RPE basal laminar (BL) space below atrophic photoreceptors, a partial descent of the external limiting membrane (ELM) (**B, D**), and a fluid pocket (**D**, light blue asterisk). The RPE layer is thinned, discontinuous or conglomerated on top of thick basal laminar deposit (fuchsia asterisks). Sloughed RPE (brown arrowheads) shows higher packing density of compressed and heterochrome granules above the RPE layer. In the sub RPE basal space, macrophages (blue arrowheads) and multi-nucleated giant cells (yellow arrowheads) adjoin soft druse material (orange asterisk) and calcific nodules (black asterisks). Bruch's membrane (BrM) is partly thinned but intact. Corresponding optical coherence tomography B-scans are shown in supplementary Figure 2.

BLamD, basal laminar deposit; BrM, Bruch's membrane; Ch, choroid; ChC, choriocapillaris; ELM, external limiting membrane; GCL, ganglion cell layer; HFL, Henle fiber layer; INL, inner nuclear layer; IPL, inner plexiform layer; IS, inner segments; NIR, near infrared reflectance; OCT, optical coherence tomography; ONL, outer nuclear layer; OPL, outer plexiform layer; OS, outer segments; RPE, retinal pigment epithelium.

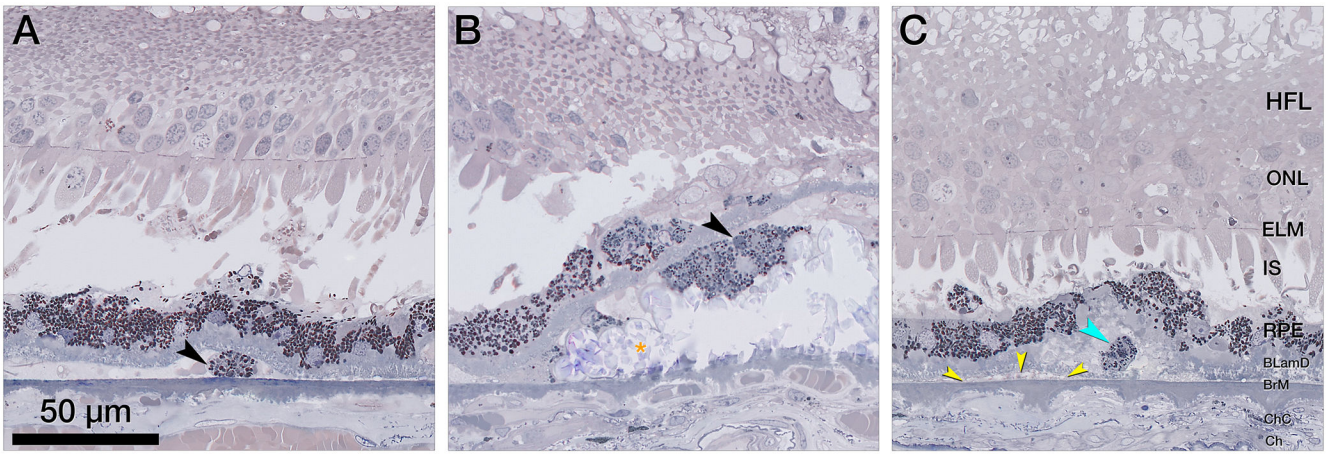

Figure 6. Retinal pigment epithelium (RPE)-originated subducted cells and granule aggregates, under the RPE cell layer

A&B. Magnified histology shows subducted retinal pigment epithelium (RPE) cells in the sub RPE- basal lamina (BL) space, with distinct content of lipofuscin and melanolipofuscin granules. Photoreceptors are short and mostly lack outer segments, Bruch's membrane (BrM) is intact, and the choriocapillaris (ChC) is atrophic. **A**. In a single subducted RPE cell (black arrowhead), granule packing density is slightly lower than in-layer RPE. **B**. A cluster of subducted cells (black arrowhead) adjacent to a calcified nodules (orange asterisk) shows granule packing density and reflectivity like in-layer RPE, which is in turn less than the cells in panel A. The subducted cells are separated from the in-layer cells by basal laminar deposit (BLamD). **C**. Subducted cells are distinct from the shedding RPE phenotype, which releases granule aggregates (teal arrowhead) into underlying BLamD; here, within a basal mound (soft drusen material). It is bounded by the native RPE-basal lamina and is therefore separate from basal linear deposit in sub-RPE-BL space (yellow arrowheads).
BLamD, basal laminar deposit; BrM, Bruch's membrane; Ch, choroid; ChC, choriocapillaris; ELM, external limiting membrane; HFL, Henle fiber layer; IS, inner segments; NIR, near infrared reflectance; OCT, optical coherence tomography; ONL, outer nuclear layer; RPE, retinal pigment epithelium sub-RPE-BL, subretinal pigment epithelium basal lamina.

Table 1.

Presence of cells in intraretinal, subretinal, and sub-RPE-BL compartments

Cellular descriptor	Intraretinal	Subretinal	sub-RPE-BL*
Cells/cellular components	130	78	136
Ectopic RPE cells/organelles	125	73	87
Non-RPE phagocytes	5†	5†	49†

Counts from right and left eyes are combined (199 glass slides total, 199 with SDD, 178 with drusen)

*sub-RPE-BL, sub retinal pigment epithelium-basal laminar space

†presumed non-RPE-phagocytes as shown in supplementary Figure 1.